Dynamics of interacting fermions in spin-dependent potentials

Andrew P. Koller,[1,2,*] Michael L. Wall,[2,*] Josh Mundinger,[3] and Ana Maria Rey[1,2]

[1] *Department of Physics, University of Colorado, Boulder, CO 80309*
[2] *JILA, NIST, Center for Theory of Quantum Matter, University of Colorado, Boulder, CO 80309*
[3] *Department of Mathematics and Statistics, Swarthmore College, 500 College Avenue, Swarthmore, PA 19081*

Recent experiments with dilute trapped Fermi gases observed that weak interactions can drastically modify spin transport dynamics and give rise to robust collective effects whose fundamental quantum origins are not well understood, including global demagnetization, macroscopic spin waves, spin segregation, and spin self-rephasing. In this work, we develop a framework for analyzing the dynamics of weakly interacting fermionic gases following a spin-dependent change of the trapping potential in regimes where standard mean-field and kinetic theory treatments are invalid. The key idea is the projection of the dynamics onto a set of lattice spin models defined on the single-particle mode space. Collective phenomena, including the global spreading of quantum correlations in real space, arise as a consequence of the long-ranged character of the spin model couplings. The spin model formulation provides a simple analytic picture of the experimental observations and illuminates the interplay between spin, motion, Fermi statistics, and interactions. Our results suggest a number of directions for future experiments in the weakly interacting regime.

The interplay between spin and motional degrees of freedom in interacting electron systems has been a long-standing research topic in condensed matter physics. Interactions can modify the behavior of individual electrons and give rise to emergent collective phenomena such as superconductivity and colossal magnetoresistance [1]. Theoretical understanding of non-equilibrium dynamics in interacting fermionic matter is limited, however, and many open questions remain. Ultracold atomic Fermi gases, with precisely controllable parameters, offer an outstanding opportunity to investigate the emergence of collective behavior in out-of-equilibrium settings.

Progress in this direction has been made by recent spin transport measurements in ultracold spin-1/2 fermionic vapors, where an initially spin polarized gas was subjected to a constant magnetic field gradient [2–4] (Fig. 1(a)), and to a spin-dependent harmonic trapping frequency [5–8], equivalent to a spatially-varying gradient. Even in the weakly interacting regime, drastic modifications of the single-particle dynamics were reported. Moreover, despite interactions being spatially local, collective phenomena were observed, including demagnetization and transverse spin-waves in the former, and a time-dependent separation (segregation) of the spin densities and spin self-rephasing in the latter. Although mean-field and kinetic theory formulations have explained some of these phenomena [8–18], a general theory capable of describing all the time scales, dramatic changes in spin polarizations, and the interplay between spin, motion, and interactions has not been developed.

In this work, we develop a theoretical framework that accounts for the coupling of spin and motional degrees of freedom in weakly interacting systems and reproduces all phenomena of the aforementioned experiments. The key idea is the representation of the state as a superposition of spin configurations which live on a lattice whose sites correspond to modes of the underlying single-particle system (see Fig. 1(b)). Within each configuration, the dynamics is described by a spin model with long-ranged couplings which generates collective quantum correlations and entanglement (see Fig. 1(c)). In the weakly interacting limit, each sector evolves independently; accumulated phase differences between sectors capture the interplay of spin and motion. Using this formulation, we gain a great deal of insight about the dynamics, and can extract analytic solutions for spin observables and correlations in several limits. Although spin models in energy space [19–24] have been used before and agreed well with experiments [5, 23, 25–29], their use was limited to pure spin dynamics (no motion). In many ways, quantum dynamics of weakly-interacting Fermi gases is less well understood than it is in the strongly-interacting limit, where interactions dominate and features of the dynam-

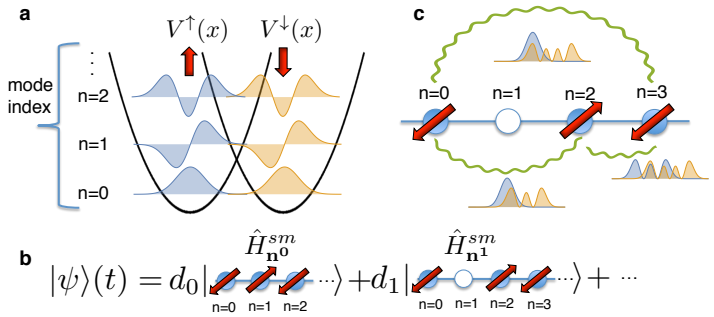

FIG. 1. (Color online) (a) Spin-↑ and spin-↓ occupy different single-particle eigenstates, labeled by mode index n. (b) After a quench, $|\psi\rangle$ is a coherent superposition of spins in many mode configurations (unoccupied modes are represented by open circles). (c) In each configuration particles are localized in mode space, with coherences capturing motional effects. Spin dynamics are generated by a spin model with long-range couplings determined by the mode overlaps (brown, shaded).

ics tend to be universal [2, 30]. Our formulation allows us to track motional degrees of freedom, compute local observables, and determine how correlations spread in real space. This opens a route for investigations of generic interacting spin-motion coupled systems beyond current capabilities. The predictions of the spin model also suggest directions for future experiments, which might, for instance, investigate the scaling of dynamical quantities or observe the collective rise of quantum correlations.

Numerical simulations of non-equilibrium fermionic matter are notoriously difficult, and for many situations no efficient algorithms presently exist. In contrast, a wide variety of powerful analytical and numerical tools have been developed for lattice quantum spin models [31–38], making a spin model description of fermionic systems potentially very useful. To demonstrate the capabilities of this approach, we use time-dependent matrix product state methods which are efficient in one-dimension [39]. We simulate systems of $N = 10 - 20$ particles; due to the coupling of spin and motion, the complexity of these simulations is similar to that of long-ranged and inhomogenous pure spin systems with $N \sim 100$ spins. We emphasize, however, that the mapping to a spin model, the corresponding analytic solutions, and the physical interpretations are valid in arbitrary dimensions. Thus the method described here will be useful for more generic cases as numerical techniques able to handle larger spin systems continue to improve.

Setup– We consider N identical fermionic atoms of mass m_a with a spin-1/2 degree of freedom $\alpha \in \{\uparrow, \downarrow\}$ trapped in a one dimensional harmonic oscillator of frequency ω, $V^0(x) = \frac{1}{2} m_a \omega^2 x^2$. The atoms experience contact s-wave collisions, parameterized by the scattering length a_s. The sample begins spin-polarized in the $\downarrow$ state, where atoms are non-interacting and populate distinct trap modes. The collective spin is then rotated to the X-axis, and the Hamiltonian quenched to the spin-dependent form $\hat{H} = \hat{H}^{sp} + \hat{H}^{int}$, ($\hbar = 1$) with

$$\hat{H}^{sp} = \sum_{\alpha} \int dx \hat{\psi}^{\dagger}_{\alpha}(x) \left(-\frac{1}{2m_a} \frac{\partial^2}{\partial x^2} + V^{\alpha}(x) \right) \hat{\psi}_{\alpha}(x),$$
$$\hat{H}^{int} = \frac{2a_s}{m_a a_{\perp}^2} \int dx \hat{\rho}_{\uparrow}(x) \hat{\rho}_{\downarrow}(x). \quad (1)$$

Here $\hat{\psi}_{\alpha}(x)$ is the fermionic field operator for spin α at point x, $\hat{\rho}_{\alpha}(x) = \hat{\psi}^{\dagger}_{\alpha}(x)\hat{\psi}_{\alpha}(x)$, and we have integrated over two transverse directions with small confinement length $a_{\perp} \ll a_H$, $a_H = (m_a \omega^2)^{-\frac{1}{2}}$. Expanding the field operators in the basis of single-particle eigenstates $\phi^{\alpha}_n(x)$ with associated creation operator $\hat{c}^{\dagger}_{n\alpha}$ and defining the interaction parameter $u_{\uparrow\downarrow} = 2a_s/(m_a a_H a_{\perp}^2)$, $\hat{H}^{int}$ becomes $u_{\uparrow\downarrow} \sum_{nmpq} A_{nmpq} \hat{c}^{\dagger}_{n\uparrow} \hat{c}_{m\uparrow} \hat{c}^{\dagger}_{p\downarrow} \hat{c}_{q\downarrow}$. The interaction parameters $A_{nmpq} = a_H \int dx \phi^{\uparrow}_n(x) \phi^{\uparrow}_m(x) \phi^{\downarrow}_p(x) \phi^{\downarrow}_q(x)$ depend on mode overlaps (Fig. 1(c)).

We consider $V^{\alpha=\uparrow,\downarrow}(x) = V^0(x) + \Delta V^{\alpha}(x)$, with $\Delta V^{\alpha}(x)$ generated by a magnetic field with a constant gradient, $\Delta V^{\alpha}(x) = \pm Bx$, or a linear gradient, $\Delta V^{\alpha}(x) = \pm \omega_B^2 m_a^2 x^2/2$. In both cases the single-particle Hamiltonian can be written as:

$$\hat{H}^{sp} = \sum_n \left[\bar{\omega}(n + 1/2)\hat{N}_n + \Delta\omega\,(n + 1/2)\,\hat{\sigma}^Z_n \right], \quad (2)$$

with $\hat{N}_n = \hat{c}^{\dagger}_{n\uparrow}\hat{c}_{n\uparrow} + \hat{c}^{\dagger}_{n\downarrow}\hat{c}_{n\downarrow}$, and $\{\hat{\sigma}^X_n, \hat{\sigma}^Y_n, \hat{\sigma}^Z_n\} \equiv \sum_{\alpha,\beta} \hat{c}^{\dagger}_{n\alpha} \vec{\sigma}_{\alpha\beta} \hat{c}_{n\beta}$ where $\vec{\sigma}$ is a vector of Pauli matrices. The constant gradient shifts the trap for spin up (down) by x_0 ($-x_0$), with $x_0 = \frac{B}{m_a \omega^2}$, but does not change the frequency; $\bar{\omega} = \omega$ and $\Delta\omega = 0$. In a noninteracting gas the $\downarrow$ and $\uparrow$ densities and the magnetization oscillate at frequency ω due to this motion [16, 40]. A linear gradient adds an additional harmonic potential term, resulting in different trap frequencies for the two spins: $\bar{\omega} = (\omega^{\uparrow} + \omega^{\downarrow})/2$ and $\Delta\omega = (\omega^{\uparrow} - \omega^{\downarrow})/2$. The noninteracting spin densities undergo a breathing motion in their respective traps, leading to oscillations in the total magnetization [40]. A finite $\Delta\omega$ causes dephasing through rotations of the magnetization in the XY plane with mode-dependent rates.

The generalized spin model approximation– The quench projects the initially polarized state, which we take to be the ground state in this work, onto the eigenmode basis of $\hat{H}^{sp}$. The state after the quench $|\psi\rangle_{t=0}$ is a coherent superposition of many product states each characterized by a set of populated modes $\mathbf{n}^i = \{\mathbf{n}^i_1, \mathbf{n}^i_2, \ldots, \mathbf{n}^i_N\}$: $|\psi\rangle_{t=0} = \sum_i d_i \bigotimes_{j=1}^{N} \left(\hat{c}^{\dagger}_{\mathbf{n}^i_j \uparrow} + \hat{c}^{\dagger}_{\mathbf{n}^i_j \downarrow} \right) |0\rangle$. The coefficients d_i are determined by the change of basis.

Our key approximation is that single particle modes either remain the same or are exchanged between two colliding atoms. Exact numerical calculations confirm the validity of this approximation in the weakly interacting regime [41]. For each set $\mathbf{n}^i$ the resulting total Hamiltonian takes the form of an XXZ spin model,

$$\hat{H}^{sm}_{\mathbf{n}^i} = \hat{H}^{sp}_{\mathbf{n}^i} + \sum_{n \neq m \in \mathbf{n}^i} \sum_{\nu = X,Y,Z} J^{\nu}_{nm} \hat{\sigma}^{\nu}_n \hat{\sigma}^{\nu}_m\,, \quad (3)$$

plus additional small density-$\hat{\sigma}^Z$ couplings [41]. Here, the Ising, $J^Z_{nm} \equiv A_{nnmm}$, and exchange, $J^X_{nm} = J^Y_{nm} = J^{\perp}_{nm} \equiv A_{nmmn}$, couplings result from the overlap between the $\uparrow$ and $\downarrow$ single-particle eigenstates (Fig. 1(c)) and are long-ranged ($\sim 1/\sqrt{|n-m|}$) [41]. In our approximation, each sector $\mathbf{n}^i$ evolves independently, but with $\mathbf{n}^i$-dependent parameters, under Eq. 3. When computing observables, we account for both the fully quantum mechanical, interaction-driven spin dynamics within each $\mathbf{n}^i$ sector, as well as single-particle dynamics from the coherences between sectors.

Spin observables– The local and collective magnetizations are given by $\hat{\vec{\mathcal{S}}}(x) = \frac{1}{2} \sum_{nm,\alpha,\beta} \phi^{\alpha}_n(x) \phi^{\beta}_m(x) \left(\hat{c}^{\dagger\alpha}_n \vec{\sigma}_{\alpha\beta} \hat{c}^{\beta}_m \right)$ and $\hat{\vec{\mathcal{S}}} = \int dx \hat{\vec{\mathcal{S}}}(x)$. Fig. 2 summarizes the results for a constant gradient with $N = 10$ [42]. At short times the collective magnetization $\langle \hat{\mathcal{S}}^X \rangle$ ((a) and (e)) exhibits characteristic

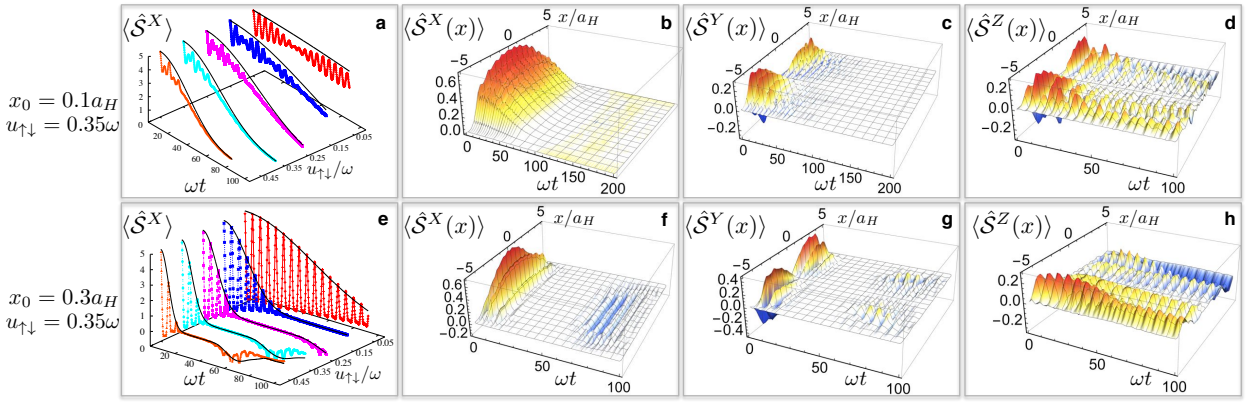

FIG. 2. (Color online) Magnetization dynamics for a constant gradient. Collective $\langle\hat{\mathcal{S}}^X\rangle$ (a) (and (e)) displays global interaction-induced demagnetization, which damps single-particle oscillations. Collective (generic) Ising solutions, black lines, give the demagnetization envelopes. Local magnetizations $\langle\hat{\mathcal{S}}^{X,Y,Z}(x)\rangle$(b-d) (and f-h) reflect similar behavior.

single-particle oscillations at frequency ω; these quickly dephase and are modulated by a global envelope with a longer time scale. Similar behavior is observed for the local magnetizations $\langle\hat{\mathcal{S}}^{X,Y,Z}(x)\rangle$ (b-d, f-h). Although the total $\langle\hat{\mathcal{S}}^{Y,Z}\rangle$ magnetizations are zero at all times, the local quantities $\langle\hat{\mathcal{S}}^{Y,Z}(x)\rangle$ evolve due to coherences between mode configurations. Their dynamics, however, are damped by interactions (Fig 2 (b-d, f-h)).

The dynamics can be understood as follows. For spin independent potentials, $J^Z_{nm} = J^\perp_{nm}$ and $\Delta\omega = 0$. The Hamiltonian $\hat{H}^{sm}_{\mathbf{n}^i}$ is SU(2) symmetric and commutes with $\hat{\vec{S}}^2$, where $\hat{\vec{S}} \equiv \frac{1}{2}\sum_n \hat{\vec{\sigma}}_n$, and so its eigenstates can be labelled by the total spin S. When a gradient is applied, the SU(2) symmetry is broken by terms $\Delta_{nm} = J^Z_{nm} - J^\perp_{nm}$ ($\Delta\omega = 0$ for a constant gradient), and the Hamiltonian can be rewritten as $\hat{H}^S_{\mathbf{n}^i} + \hat{H}^\delta_{\mathbf{n}^i}$, where

$$\hat{H}^S_{\mathbf{n}^i} = E_{\mathbf{n}^i} - \frac{u_{\uparrow\downarrow}}{4}\sum_{n\neq m\in\mathbf{n}^i}\left[J^\perp_{nm}\vec{\sigma}_n\cdot\vec{\sigma}_m + \bar{\Delta}\hat{\sigma}^Z_n\hat{\sigma}^Z_m\right],$$
$$\hat{H}^\delta_{\mathbf{n}^i} = -\frac{u_{\uparrow\downarrow}}{4}\sum_{n\neq m\in\mathbf{n}^i}\delta_{nm}\hat{\sigma}^Z_n\hat{\sigma}^Z_m, \qquad (4)$$

$E_{\mathbf{n}^i} = \bar{\omega}\sum_{n\in\mathbf{n}^i}(n+1/2)$ is a constant, $\bar{\Delta}$ is the average value of Δ_{nm}, and $\delta_{nm} = \Delta_{nm} - \bar{\Delta}$. $\hat{H}^S_{\mathbf{n}^i}$ commutes with $\hat{\vec{S}}^2$ so only $\hat{H}^\delta_{\mathbf{n}^i}$ induces transitions between manifolds of different S. For a sufficiently weak gradient, and $\delta_{nm} \ll J^\perp_{nm}$, a large energy gap G, which we call the *Dicke gap*, opens between the $S = N/2$ "Dicke" manifold and the $S = (N/2-1)$ manifold [41]. The system remains in the Dicke manifold when terms in $\hat{H}^\delta_{\mathbf{n}^i}$ are small compared to this gap, and dynamics resulting from the collective Ising term in $\hat{H}^S_{\mathbf{n}^i}$ is given by $\langle\hat{S}^X\rangle_{\mathbf{n}^i} = \frac{N}{2}\cos^{N-1}\left(u_{\uparrow\downarrow}\bar{\Delta}t\right)$, and $\langle\hat{S}^{Y,Z}\rangle_{\mathbf{n}^i} = 0$. Since the interaction parameters J^Z_{nm} and $J^\perp_{nm}$ vary slowly with parameter index, the dynamics of $\langle\hat{S}^X\rangle_{\mathbf{n}^i}$ is approximately the same for all i, and a single configuration $\mathbf{n}^0 \equiv \{0, 1, \cdots N-1\}$ well reproduces the demagnetization envelope (Fig. 2(a)).

For strong gradients, mode-exchange processes are suppressed and only mode-preserving processes remain significant. The effective interaction Hamiltonian becomes a generic Ising model $\hat{H}^{\text{Ising}}_{\mathbf{n}^i} = -\frac{u_{\uparrow\downarrow}}{4}\sum_{n\neq m\in\mathbf{n}^i} J^Z_{nm}\hat{\sigma}^Z_n\hat{\sigma}^Z_m$, which also admits a simple expression for the spin magnetization dynamics [35–38] $\langle\hat{S}^X\rangle_{\mathbf{n}^i} = \sum_{n\in\mathbf{n}^i}\prod_{m\neq n\in\mathbf{n}^i}\cos\left(u_{\uparrow\downarrow}J^Z_{nm}t\right)$. In this limit the demagnetization envelope can be captured by the $\mathbf{n}^0$ realization of the generic Ising solution (Fig. 2(e)).

Using a perturbation analysis, the short time dynamics of the XXZ Hamiltonian [43] is given by $\langle\hat{S}^X\rangle = \langle\hat{S}^X\rangle_{t=0}\left(1-(t/\tau_M)^2\right) + O(t^3)$, where τ_M is defined as the demagnetization time. By analyzing the scaling of the interaction parameters we find that $\tau_M \sim \left(Nu_{\uparrow\downarrow}x_0^2\right)^{-1}$, a prediction that agrees well the numerical scaling $\sim u^{-1}_{\uparrow\downarrow}x_0^{-2}N^{-0.823}$ [41]. Similar behavior was reported in Ref. [2] in the weakly-interacting regime where the demagnetization rate scaled roughly with the interaction strength. Although the experiment was conducted in two dimensions, we expect the scaling analysis to remain valid due to the collective character of the dynamics. We note that the spin echo pulse applied in Refs. [2, 3] modifies the single-particle physics [40], but does not affect the interaction-induced collective demagnetization. Investigating these scalings in the weakly-interacting regime is a possible direction for future experiments.

Fig. 3 (a) [(b)] shows the numerically-obtained total magnetization vs. interactions for weaker [stronger] linear gradient. In a weak gradient the magnetization remains nearly constant for a sufficiently strong gradient, and the collective spin dynamics is a global precession in the XY plane (inset). This self-rephasing effect was experimentally reported in Ref. [5]. The Z magnetization exhibits a clear, long-time spatial separation of the spin densities (spin segregation): the $\uparrow$ ($\downarrow$) atoms accumulate at the center (edge) of the cloud. Spin segregation in fermionic gases, first reported in Ref. [7], occurred at

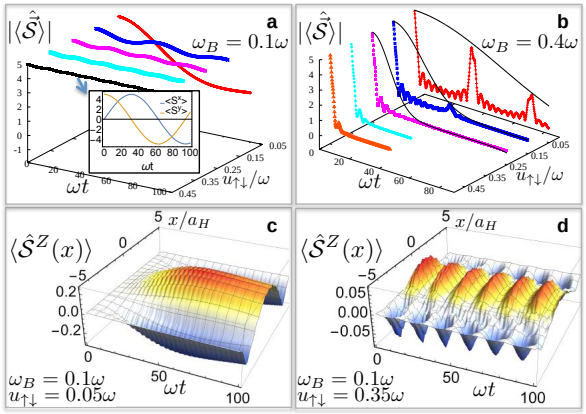

FIG. 3. (Color online) Magnetization dynamics for a linear gradient. (a) As interactions increase, $\langle \hat{\vec{\mathcal{S}}} \rangle$ precesses collectively in the XY plane (inset), leading to self-rephasing (constant $|\langle \hat{\vec{\mathcal{S}}} \rangle|$). (b) For a stronger gradient, demagnetization envelopes (black lines) are predicted by the generic Ising solutions. The local $\hat{\mathcal{S}}^Z(x)$ magnetization exhibits spin segregation oscillations (c,d) at a rate proportional to the interaction strength.

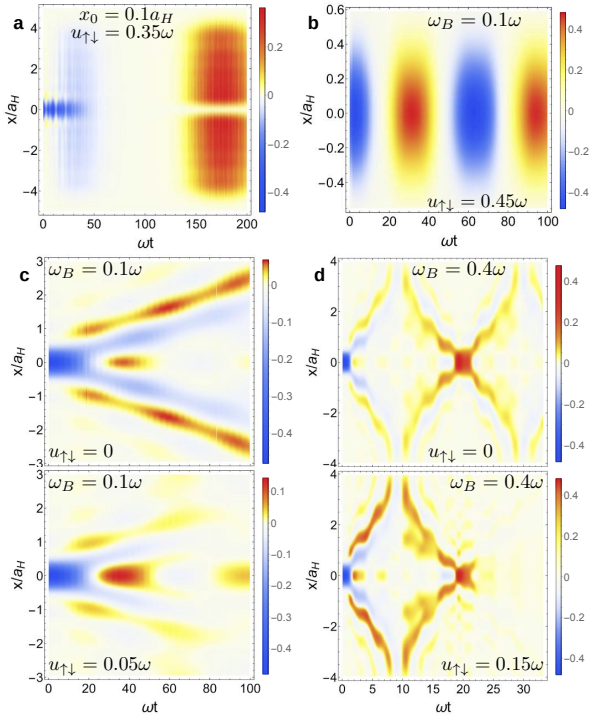

FIG. 4. (Color online) Real part of connected correlation functions $\mathrm{Re}\left[G^{++}(x,0;t)\right]$. (a) In a weak constant gradient, correlations grow collectively. (b) In a linear gradient in the self-rephasing regime, G^{++} exhibits a collective phase rotation. For weaker interactions or stronger gradients (c, d), interactions collectively damp the correlations arising from quantum statistics ($u_{\uparrow\downarrow} = 0$, upper panels).

timescales set by the mean interaction energy, and reversed sign when interactions were switched from attractive to repulsive. We observe this behavior in our numerical simulations, and the spin model provides a simple interpretation.

For a weak gradient, the single-particle term $\propto \Delta\omega$ gives rise to the largest inhomogeneity. In this limit the Hamiltonian simplifies to $-\frac{u_{\uparrow\downarrow}}{4}\sum_{n\neq m} J^{\perp}_{nm}\vec{\sigma}_n\cdot\vec{\sigma}_m + \sum_n \Delta\omega(n+\frac{1}{2})\hat{\sigma}^Z_n$. When $\Delta\omega\langle n\rangle \ll G$, where G is the Dicke gap and $\langle n\rangle$ is the average mode occupation, the system remains in the Dicke manifold. After projecting $\hat{H}^{sp}$ onto the Dicke states, the dynamics of total spin observables is just a collective precession in the XY plane of the generalized Bloch vector, i.e $\langle \hat{S}^{\pm}(t)\rangle = \langle \hat{S}^{\pm}(0)\rangle e^{\pm 2it(\langle n\rangle+\frac{1}{2})\Delta\omega}$, with $\hat{S}^{\pm} = \hat{S}^X \pm i\hat{S}^Y$, as seen in Fig. 3(a, inset). At leading order the system stays entirely in the Dicke manifold, $\langle \hat{S}^Z\rangle = 0$, and spin segregation does not occur. However, the gradient generates a coupling between the $S = N/2$ and the $S = (N/2-1)$ states, which induces Rabi-type oscillations with lowest-order angular frequency $\sim G$ [41]. The gap G is also a measure of the mean-field interaction energy $\sim N\bar{J}^{\perp}u_{\uparrow\downarrow}$ for fully collective interactions. For weaker interactions or larger inhomogeneities, the oscillations decay due to population of other spin manifolds, e.g., $S = (N/2-2)$. For stronger gradients the condition $\Delta\omega\langle n\rangle \ll G$ is violated, and the demagnetization envelope is instead given by the generic Ising solutions (Fig. 3(b)).

Correlations– Our approach can be used to compute higher-order correlations, such as the $G^{++}(x,x') = \langle \hat{\mathcal{S}}^+(x)\hat{\mathcal{S}}^+(x')\rangle - \langle \hat{\mathcal{S}}^+(x)\rangle\langle \hat{\mathcal{S}}^+(x')\rangle$ correlator shown in Fig. 4. Although the system is initially non-interacting, $G^{++}(t=0)$ shows finite anti-bunching correlations near $x \sim x'$ arising from Fermi statistics (mode entanglement) [44, 45]. At later times, correlations behave collectively, a distinct consequence of the long-range character of the spin coupling parameters [46–50].

For a weak constant gradient, the collective Ising model provides a good characterization of the correlation dynamics. For each spin configuration $G^{++}_{\mathbf{n}^i}(x,x';t) = f^i_1(x,x')\cos^{N-2}\left(2u_{\uparrow\downarrow}\bar{\Delta}t\right) - f^i_2(x,x')\cos^{2N-2}\left(u_{\uparrow\downarrow}\bar{\Delta}t\right)$, where the functions $f^i_{1,2}(x,x')$ depend on the set of populated modes [41]. G^{++} peaks at the time when the system has completely demagnetized (Fig. 4(a)). For a pure spin system with a collective Ising Hamiltonian, the state at this time is a Schrödinger-cat state [51, 52]. For the linear gradient in the self-rephasing regime, we observe collective precession of G^{++} (Fig. 4(b)). As interactions decrease or the inhomogeneity increases, correlations are strongly affected by the interplay between single-particle dynamics and interactions (Fig. 4(c, d)). Mode entanglement tends to cause an almost linear spreading of the correlations with time [53–55], while interactions tend to globally distribute and damp those correlations. Current experiments are in position to

confirm these predictions.

Outlook– We have discussed an approach to model the interplay of motional and spin degrees of freedom in weakly interacting fermionic systems in spin-dependent potentials. Simulations reproduce several collective dynamical phenomena that were recently observed in cold gas experiments, and we can understand the physics behind these effects with simple considerations. While we focused on 1D systems to enable a rigorous comparison of analytical predictions to unbiased numerical simulations, we emphasize that the model, analytic solutions, and theoretical pictures developed are general. For larger systems and in higher dimensions, methods such as the discrete truncated Wigner approximation [32–34], which is uncontrolled but performed well in benchmark tests [56], can be used to make direct comparison with experiments. Our formulation may also be useful for modeling another class of spin transport experiments [30, 57], in which dynamics is induced by an initial spatial separation of the spin populations. While our model only works in the weakly interacting limit, it has recently been pointed out that local spin models can be formulated in the opposite, strong coupling regime [58–61]. It could be interesting to investigate ways to connect these formulations.

ACKNOWLEDGEMENTS

We thank J. E. Thomas, K. R. A. Hazzard, A. Pikovski, and J. Schachenmayer for useful discussions, and P. Romatschke, J. Bohnet, and M. Gärttner for comments on the manuscript. This work was supported by JILA-NSF-PFC-1125844, NSF-PIF- 1211914, ARO, AFOSR, and AFOSR-MURI. AK was supported by the Department of Defense through the NDSEG program. MLW thanks the NRC postdoctoral fellowship program for support.

---

* A.P.K. and M.L.W. contributed equally to this work.

[1] A. P. Ramirez, Journal of Physics: Condensed Matter **9**, 8171 (1997).
[2] M. Koschorreck, D. Pertot, E. Vogt, and M. Kohl, Nature Physics **9**, 405 (2013).
[3] A. B. Bardon, S. Beattie, C. Luciuk, W. Cairncross, D. Fine, N. S. Cheng, G. J. A. Edge, E. Taylor, S. Zhang, S. Trotzky, and J. H. Thywissen, Science **344**, 722 (2014).
[4] S. Trotzky, S. Beattie, C. Luciuk, S. Smale, B. Bardon, A. T. Enss, E. Taylor, S. Zhang, and H. Thywissen, J. Phys. Rev. Lett. **114**, 015301 (2015).
[5] C. Deutsch, F. Ramirez-Martinez, C. Lacroûte, F. Reinhard, T. Schneider, J. N. Fuchs, F. Piéchon, F. Laloë, J. Reichel, and P. Rosenbusch, Phys. Rev. Lett. **105**, 020401 (2010).
[6] H. J. Lewandowski, D. M. Harber, D. L. Whitaker, and E. A. Cornell, Phys. Rev. Lett. **88**, 070403 (2002).
[7] X. Du, L. Luo, B. Clancy, and J. E. Thomas, Phys. Rev. Lett. **101**, 150401 (2008).
[8] X. Du, Y. Zhang, J. Petricka, and J. E. Thomas, Phys. Rev. Lett. **103**, 010401 (2009).
[9] J. N. Fuchs, D. M. Gangardt, and F. Laloë, Phys. Rev. Lett. **88**, 230404 (2002).
[10] J. E. Williams, T. Nikuni, and C. W. Clark, Phys. Rev. Lett. **88**, 230405 (2002).
[11] A. S. Bradley and C. W. Gardiner, Journal of Physics B: Atomic, Molecular and Optical Physics **35**, 4299 (2002).
[12] S. S. Natu and E. J. Mueller, Phys. Rev. A **79**, 051601 (2009).
[13] U. Ebling, A. Eckardt, and M. Lewenstein, Phys. Rev. A **84**, 063607 (2011).
[14] G. M. Bruun, New Journal of Physics **13**, 035005 (2011).
[15] F. Piéchon, J. N. Fuchs, and F. Laloë, Phys. Rev. Lett. **102**, 215301 (2009).
[16] J. Xu, Q. Gu, and E. J. Mueller, Phys. Rev. A **91**, 043613 (2015).
[17] O. Goulko, F. Chevy, and C. Lobo, Phys. Rev. Lett. **111**, 190402 (2013).
[18] T. Enss, Phys. Rev. A **91**, 023614 (2015).
[19] M. O. Oktel, T. C. Killian, D. Kleppner, and L. S. Levitov, Phys. Rev. A **65**, 033617 (2002).
[20] K. Gibble, Physical Review Letters **103**, 113202 (2009).
[21] A. M. Rey and A. V. Gorshkov and C. Rubbo, Phys. Rev. Lett. **103**, 260402 (2009).
[22] Z. H. Yu and C. J. Pethick, Phys. Rev. Lett. **104**, 010801 (2010).
[23] E. Hazlett, Y. Zhang, R. Stites, K. Gibble, and K. M. O'Hara, Phys. Rev. Lett. **110**, 160801 (2013).
[24] M. E. Beverland, G. Alagic, M. J. Martin, A. P. Koller, A. M. Rey, and A. V. Gorshkov, arXiv:1409.3234 (20014).
[25] M. D. Swallows, M. Bishof, Y. G. Lin, S. Blatt, M. J. Martin, A. M. Rey, and J. Ye, Science **331**, 1043 (2011).
[26] W. Maineult, C. Deutsch, K. Gibble, J. Reichel, and P. Rosenbusch, Phys. Rev. Lett. **109**, 020407 (2012).
[27] M. J. Martin, M. Bishof, M. D. Swallows, X. Zhang, C. Benko, J. von Stecher, A. V. Gorshkov, A. M. Rey, and J. Ye, Science **341**, 632 (2013).
[28] H. Pechkis, J. Wrubel, A. Schwettmann, P. Griffin, R. Barnett, E. Tiesinga, and P. Lett, Phys. Rev. Lett. **111**, 025301 (2013).
[29] B. Yan, S. A. Moses, B. Gadway, J. P. Covey, K. R. A. Hazzard, A. M. Rey, D. S. Jin, and J. Ye, Nature **501**, 521 (2013).
[30] A. Sommer, M. Ku, G. Roati, and M. W. Zwierlein, Nature **472**, 201 (2011).
[31] U. Schollwöck, Annals of Physics **326**, 96 (2011), january 2011 Special Issue.
[32] A. Polkovnikov, Annals of Physics **325**, 1790 (2010).
[33] J. Schachenmayer, A. Pikovski, and A. M. Rey, Phys. Rev. X **5**, 011022 (2015).
[34] L. Pucci, A. Roy, and M. Kastner, arXiv:1510.03768 (20015).
[35] G. G. Emch, Journal of Mathematical Physics **7**, (1966).
[36] C. Radin, Journal of Mathematical Physics **11**, (1970).
[37] M. Kastner, Phys. Rev. Lett. **106**, 130601 (2011).
[38] M. Foss-Feig, K. R. A. Hazzard, J. J. Bollinger, and A. M. Rey, Phys. Rev. A **87**, 042101 (2013).
[39] The matrix product state studies of the main text were performed using extensions of the open source MPS library [62, 63], and are described further in the supplement [41].

[40] A. P. Koller, J. Mundinger, M. L. Wall, and A. M. Rey, Phys. Rev. A **92**, 033608 (2015).
[41] A. P. Koller, M. L. Wall, J. Mundinger, and A. M. Rey, Supplemental material (2015).
[42] All simulations displayed in figures in the main text are for $N = 10$.
[43] K. R. A. Hazzard, M. van den Worm, M. Foss-Feig, S. R. Manmana, E. G. Dalla Torre, T. Pfau, M. Kastner, and A. M. Rey, Phys. Rev. A **90**, 063622 (2014).
[44] V. Vedral, Open Physics **1**, 289 (2003).
[45] S. Clark, C. M. Alves, and D. Jaksch, New Journal of Physics **7**, 124 (2005).
[46] P. Hauke and L. Tagliacozzo, Physical review letters **111**, 207202 (2013).
[47] J. Schachenmayer, B. Lanyon, C. Roos, and A. Daley, Physical Review X **3**, 031015 (2013).
[48] J. Eisert, M. van den Worm, S. R. Manmana, and M. Kastner, Physical review letters **111**, 260401 (2013).
[49] Z.-X. Gong, M. Foss-Feig, S. Michalakis, and A. V. Gorshkov, Physical review letters **113**, 030602 (2014).
[50] P. Richerme, Z.-X. Gong, A. Lee, C. Senko, J. Smith, M. Foss-Feig, S. Michalakis, A. V. Gorshkov, and C. Monroe, Nature **511**, 198 (2014).
[51] M. Kitagawa and M. Ueda, Physical Review A **47**, 5138 (1993).
[52] T. Opatrnỳ and K. Mølmer, Physical Review A **86**, 023845 (2012).
[53] E. Lieb and R. D., Commun. Math. Phys. **28**, 251 (1972).
[54] B. Nachtergaele, Y. Ogata, and R. Sims, Journal of statistical physics **124**, 1 (2006).
[55] M. Cheneau, P. Barmettler, D. Poletti, M. Endres, P. Schauß, T. Fukuhara, C. Gross, I. Bloch, C. Kollath, and S. Kuhr, Nature **481**, 484 (2012).
[56] J. Schachenmayer, A. Pikovski, and A. M. Rey, New Journal of Physics **17**, 065009 (2015).
[57] D. Niroomand, S. D. Graham, and J. M. McGuirk, Phys. Rev. Lett. **115**, 075302 (2015).
[58] F. Deuretzbacher, D. Becker, J. Bjerlin, S. M. Reimann, and L. Santos, Phys. Rev. A **90**, 013611 (2014).
[59] A. G. Volosniev, D. V. Fedorov, A. S. Jensen, M. Valiente, and N. T. Zinner, Nat Commun **5**, (2014).
[60] L. Yang, L. Guan, and H. Pu, Physical Review A **91**, 043634 (2015).
[61] L. Yang and X. Cui, arXiv preprint arXiv:1510.06087 (2015).
[62] Open Source MPS, http://sourceforge.net/projects/openmps/.
[63] M. L. Wall and L. D. Carr, New Journal of Physics **14**, 125015 (2012).
[64] A. P. Koller, M. Beverland, A. V. Gorshkov, and A. M. Rey, Phys. Rev. Lett. **112**, 123001 (2014).
[65] J. S. Krauser, U. Ebling, N. Flschner, J. Heinze, K. Sengstock, M. Lewenstein, A. Eckardt, and C. Becker, Science **343**, 157 (2014).
[66] M. P. Zaletel, R. S. K. Mong, C. Karrasch, J. E. Moore, and F. Pollmann, Phys. Rev. B **91**, 165112 (2015).
[67] G. M. Crosswhite, A. C. Doherty, and G. Vidal, Phys. Rev. B **78**, 035116 (2008).
[68] B. Pirvu, V. Murg, J. I. Cirac, and F. Verstraete, New Journal of Physics **12**, 025012 (2010).

Supplemental material for "Dynamics of interacting fermions in spin-dependent potentials"

In this supplemental material we discuss the generalized spin model approximation and its range of validity, explain in detail how spin segregation arises in a many body system, present dynamical scaling results, and discuss our numerical methods.

THE GENERALIZED SPIN MODEL APPROXIMATION: VALIDITY AND DISCUSSION

The spin model approximation ignores interaction-induced changes of the single-particle motional quantum states and is thus only valid when interactions are weak compared to the harmonic oscillator energy spacing, $u_{\uparrow\downarrow} \ll \omega$. The range of validity of this approximation is essentially when the system is "collisionless," although the exact crossover to the collisional regime depends not only on the interaction energy but also on the strength of the gradient for the quenches discussed in this work [16]. When interactions are weak compared to the oscillator spacing, collisional processes that do not conserve single particle energy can safely be ignored. However, processes that *do* conserve single particle energy, but at the same time change the populated single particle modes, i.e. "resonant" mode changes, can be important for a harmonic trap [64]. While there are a large number of such terms in a harmonic trap due to the equal spacing of energy levels, realistic optical traps in cold atom experiments include anharmonicity which breaks these degeneracies. In higher dimensions, the non-separability of the trapping potential suppresses the redistribution of energy modes in the transverse directions. When the energy differences due to anharmonicity and non-separability of the trapping potential are larger than the interaction strength, these terms will be suppressed. This was shown to be the case for example in Refs. [23, 27, 28] where a pure spin model accurately described the experimental observations. Additionally, at very low temperatures, Pauli blocking can partially prevent mode changing collisions for a spin-polarized sample, as recently observed in Ref. [65]. However, even in a spin-polarized gas, spin- and mode-changing processes may occur, resulting in a doubly occupied mode.

We compare exact diagonalization of the full Hamiltonian, including all interaction-induced mode changes, to the spin model prediction for a small number of particles to test its validity. The results are shown in Fig. 5. Panel (a)

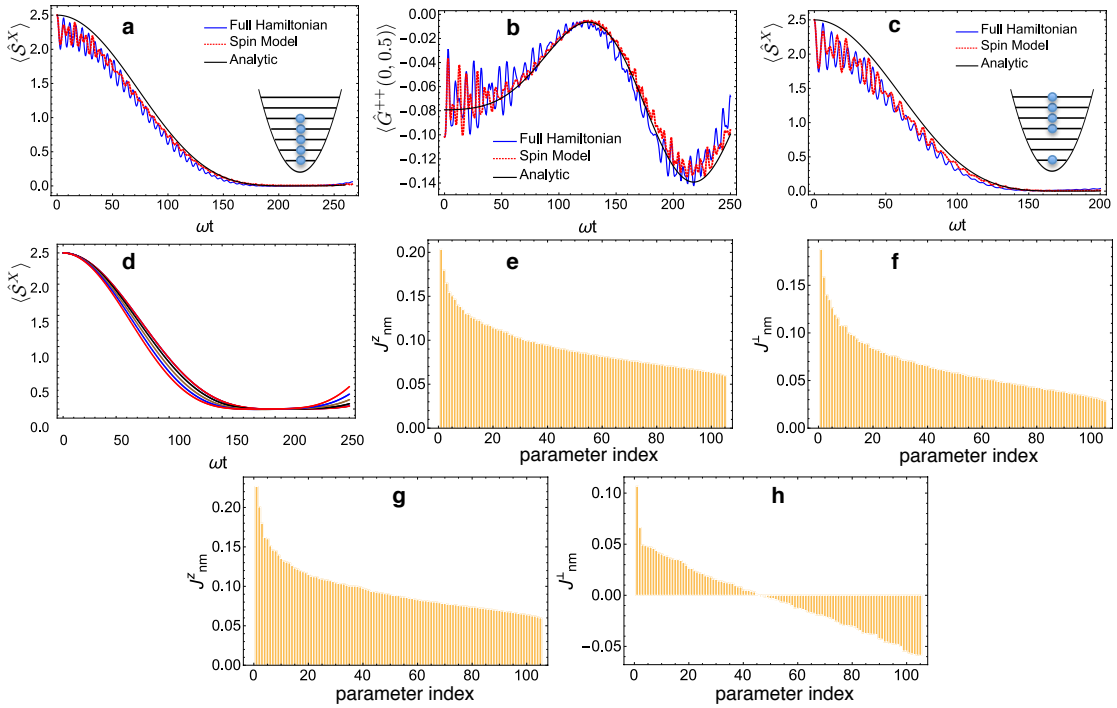

FIG. 5. Spin model approximation vs. full Hamiltonian for 5 particles with $x_0 = 0.1a$ and $u_{\uparrow\downarrow} = 0.35\omega$. (a) $\langle \hat{\mathcal{S}}^X \rangle$ quench dynamics for initial modes {0,1,2,3,4}, representing a zero temperature gas, along with (b) the connected correlator $G^{++}(x = 0, x' = 0.5a_H)$. Single-particle oscillations is damped by interactions, and the long time dynamics is well-reproduced by the spin model approximation with decay envelope given by the collective Ising solutions. (c) Dynamics for initial modes {0,3,4,5,6} representing a more dilute gas. (d) Dynamics of a pure XXZ spin Hamiltonian with the same parameters, for each of the lowest "one-hole" mode configurations. The dynamics of each configuration is very similar, explaining why the dynamics of a quench – involving many configurations – can be approximated by a single configuration. The interaction parameters vary slowly with parameter index, as shown in (e,f) for $x_0 = 0.1a_H$ and (g,h) for $x_0 = 0.3a_H$.

shows the dynamics of $\langle \hat{\mathcal{S}}^X \rangle$ for five particles following a quench of a constant gradient with $x_0 = 0.1a$ and $u_{\uparrow\downarrow} = 0.35\omega$. The quench induces single-particle dynamics which we observe as fast oscillations at the trapping period. In the spin model approximation, these oscillations are modified due to interactions and become damped at long times. The long time demagnetization and damping of single particle oscillations are well captured by the spin model approximation. Also plotted is the analytic solution for the collective Ising model which captures the demagnetization envelope. Fig. 5(c) shows the dynamics for a different initial mode configuration – $\{0, 3, 4, 5, 6\}$ – where Pauli blocking would not prevent several resonant mode changing processes. For instance, the process $(n = 0, m = 3) \to (n = 1, m = 2)$ is resonant. The spin model approximation works well even in this case.

The initial state after a quench is a superposition of many different product states of spins, in different mode configurations labeled $\mathbf{n}^i$. Because the interaction parameters vary slowly with parameter index, each $\mathbf{n}^i$ has similar interaction parameters and similar dynamics. Fig. 5(d) shows the dynamics for 5 spins evolved under a pure XXZ Hamiltonian, with the same conditions as the dynamics in Fig. 5(a). Each curve represents a different "one-hole" mode configuration of five spins that differs from $\mathbf{n}^0 \equiv \{0, 1, 2, 3, 4\}$ by exactly one mode ($\mathbf{n}^0$ dynamics is also shown). For instance, the initially occupied modes could be $\{0, 1, 2, 3, 5\}$ or $\{0, 1, 2, 4, 5\}$, etc. All these configurations contribute to the dynamics after a quench. Since they all have similar dynamics, however, we only need to consider the $\mathbf{n}^0$ configuration to reproduce the demagnetization envelope. The slow variation of the interaction parameters is illustrated in Fig. 5(e,f) where we plot the value of all the parameters J^Z_{nm} and $J^\perp_{nm}$ for modes $n, m = 0$ through $n, m = 15$, sorted by value and labeled by a parameter index. In Fig. 5(g,h) we show that the interaction parameters also vary slowly for a stronger gradient, $x_0 = 0.3a_H$. The slow variation of interaction parameters also helps explain why mode changes are relatively unimportant: a mode change simply evolves the system to another mode configuration where the dynamics are nearly the same.

The collective Ising solution gives the connected correlation function studied in the main text as

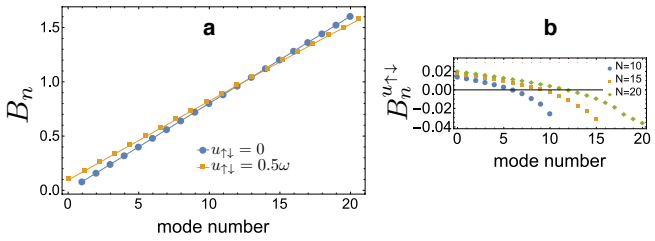

FIG. 6. (a) Magnitude of of the total field $B_n\hat{\sigma}_n^Z$, which contains both single particle ($B^{sp}\hat{\sigma}_n^Z$) and interaction ($B_n^{u_{\uparrow\downarrow}}\hat{\sigma}_n^Z$) terms, for a linear gradient with $\Delta\omega = 0.08\omega$. Even for strong interactions ($u_{\uparrow\downarrow} = 0.5\omega$), the Hamiltonian is not significantly modified by the interaction-induced terms $B_n^{u_{\uparrow\downarrow}}$ which appear when $J_{nm}^Z \neq J_{mn}^Z$. (b) For $u_{\uparrow\downarrow} = 0.5\omega$ the $B_n^{u_{\uparrow\downarrow}}$ terms do not grow with particle number.

$G^{++}_{\mathbf{n}^i}(x,x';t) = f_1^i(x,x')\cos^{N-2}\left(2u_{\uparrow\downarrow}\bar{\Delta}t\right) - f_2^i(x,x')\cos^{2N-2}\left(u_{\uparrow\downarrow}\bar{\Delta}t\right)$, where the functions $f_{1,2}^i(x,x')$ are given by

$$f_1^i(x,x') = \frac{1}{4}\sum_{nm\in\mathbf{n}^i}\left(\phi_n^\uparrow(x)\phi_n^\downarrow(x)\phi_m^\uparrow(x')\phi_m^\downarrow(x') - \phi_n^\uparrow(x)\phi_n^\downarrow(x')\phi_m^\uparrow(x')\phi_m^\downarrow(x)\right),$$
$$f_2^i(x,x') = \frac{1}{4}\sum_{nm\in\mathbf{n}^i}\phi_n^\uparrow(x)\phi_n^\downarrow(x)\phi_m^\uparrow(x')\phi_m^\downarrow(x'). \tag{S1}$$

In Fig. 5(b) we show the connected correlator $G^{++}(x,x')$ evaluated at $x = 0, x' = 0.5a_H$, along with the analytic solution for the $\mathbf{n}^0$ mode configuration. The spin model approximation and analytic solution do an excellent job of reproducing the dynamics of the correlation function. For stronger gradients where the generic Ising model is a better description of the dynamics,

$$G^{++}_{\mathbf{n}^i}(x,x';t) = \frac{1}{4}\sum_{n,m\in\mathbf{n}^i}\left(\phi_n^\uparrow(x)\phi_n^\downarrow(x)\phi_m^\uparrow(x')\phi_m^\downarrow(x') - \phi_n^\uparrow(x)\phi_n^\downarrow(x')\phi_m^\uparrow(x')\phi_m^\downarrow(x)\right)\prod_{p\neq n,m\in\mathbf{n}^i}\cos\left(J_{np}^Z t + J_{mp}^Z t\right)$$
$$-\frac{1}{4}\left[\sum_{n\in\mathbf{n}^i}\left(\phi_n^\uparrow(x)\phi_n^\downarrow(x)\right)\prod_{p\neq n\in\mathbf{n}^i}\cos\left(J_{np}^Z t\right)\right]\left[\sum_{n\in\mathbf{n}^i}\left(\phi_n^\uparrow(x')\phi_n^\downarrow(x')\right)\prod_{p\neq n\in\mathbf{n}^i}\cos\left(J_{np}^Z t\right)\right]. \tag{S2}$$

For a linear gradient, the direct interaction integrals are not symmetrical under mode exchange: $J_{nm}^Z \neq J_{mn}^Z$. The spin model Hamiltonian includes terms $\hat{H}^{as} = \frac{u_{\uparrow\downarrow}}{8}\sum_{n\neq m}\left(J_{nm}^Z - J_{mn}^Z\right)\left(\hat{\sigma}_n^Z\hat{N}_m - \hat{\sigma}_m^Z\hat{N}_n\right)$, where $\hat{N}_n = \hat{N}_n^\uparrow + \hat{N}_n^\downarrow$ and $\hat{N}_n^\alpha = \hat{c}_{n\alpha}^\dagger\hat{c}_{n\alpha}$. These terms, when summed over the index m, represent an inhomogeneous magnetic field: $\sum_m \hat{H}^{as} = \sum_n B_n^{u_{\uparrow\downarrow}}\hat{\sigma}_n^Z$. This combines with the single particle field $B_n^{sp} = \Delta\omega(n+1/2)$ to yield a total $\hat{\sigma}_n^Z$ field $B_n\sigma_n^Z$, where $B_n = B_n^{sp} + B_n^{u_{\uparrow\downarrow}}$. We find that even for relatively strong interactions ($u_{\uparrow\downarrow} = 0.5\omega$) $B_n^{u_{\uparrow\downarrow}} \ll B_n^{sp}$ for all n, as illustrated in Fig. 6, so these additional terms can be neglected. Additionally, $B_n^{u_{\uparrow\downarrow}}$ does not grow with particle number. Although these terms are not essential for the large-scale features of the dynamics, for completeness we include them in numerical simulations.

BEHAVIOR OF THE DICKE GAP G

We will now discuss the behavior of the gap between the spin-$N/2$ ("Dicke states") and spin-$(N/2-1)$ ("spin wave states"), referred to as the Dicke gap G in the main text, for a general Heisenberg model of the form $\hat{H} = -\frac{1}{4}\sum_{q\neq q'} J_{qq'}\hat{\vec{\sigma}}_q\cdot\hat{\vec{\sigma}}_{q'}$. The only condition we impose is that the coupling matrix $\mathbb{J}$ is real, for compactness of the resulting formulas, and because all couplings considered in this work are real. Noting that the diagonal terms of $\mathbb{J}$ only contribute an overall constant to the energy and hence do not affect the Dicke gap, they can be ignored. By direct calculation, the energy of the (degenerate) Dicke states, defined as $|N/2,m_z\rangle = \sqrt{\binom{N}{\frac{N}{2}+m_z}^{-1}}\left(\sum_{i=1}^N \hat{S}_i^+\right)^{\frac{N}{2}+m_z}|\downarrow\ldots\downarrow\rangle$, with m_z the magnetization, is $E_{\text{Dicke}} = \langle N/2,m_z| - \frac{1}{4}\sum_{q\neq q'} J_{qq'}\hat{\vec{\sigma}}_q\cdot\hat{\vec{\sigma}}_{q'}|N/2,m_z\rangle = -\sum_{q\neq q'} J_{q,q'}/4$. Because of the SU(2) spin-rotation symmetry of $\hat{H}$, the Dicke states are guaranteed to be eigenstates. The spin-wave states, which span the total spin-$(N/2-1)$ manifold, can be defined in terms of the Dicke states as $|N/2-1,m_z,k\rangle =$

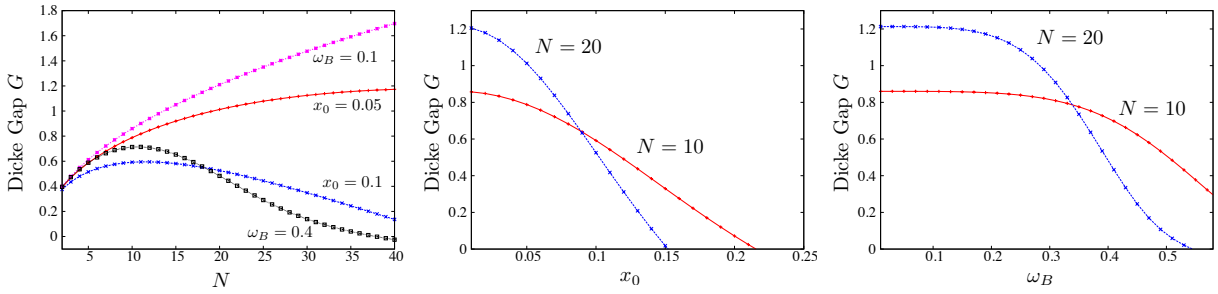

FIG. 7. Scaling of the Dicke gap G with magnetic field gradient and particle number. (Left panel) Scaling of the Dicke gap with particle number for constant gradients of strength $x_0 = 0.05$ and 0.1 and linear gradients of strength $\omega_B = 0.1$ and 0.4 (all quantities are measured in oscillator units). All gaps increase with N to a certain gradient-dependent critical value and then decrease, with larger gaps for smaller gradients. (Right panels) Scaling of the Dicke gap at fixed particle number $N = 10$ and 20 with the constant (center panel) or linear (right panel) gradient strength. The gap closes for weaker gradient as the particle number increases, demonstrating that larger particle numbers require smaller gradients to be in the near-Heisenberg regime. For even smaller gradients, the gap increases with particle number, more effectively enforcing collective behavior.

$\sqrt{\frac{(N-1)}{\left(\frac{N}{2}-m_z+1\right)\left(\frac{N}{2}-m_z\right)}}\sum_{n=1}^{N} e^{2\pi i k n/N}\hat{S}_n^+|N/2, m_z-1\rangle$, where $k = 1, \ldots, N-1$. In the case of a translationally invariant Heisenberg coupling $J_{q,q'} = J_{|q-q'|}$ with $|q-q'|$ the chordal distance, the spin wave states as stated are eigenstates of $\hat{H}$, but when the interactions are not translationally invariant (as is the case for the spin models discussed in this work), the spin wave states only form a basis for the spin-$(N/2-1)$ subspace. Straightforward calculations lead to the matrix elements of the Hamiltonian in this subspace:

$$\langle \frac{N}{2}-1, m_z, k| -\frac{1}{4}\sum_{q\neq q'} J_{q,q'}\hat{\vec{\sigma}}_q\cdot\hat{\vec{\sigma}}_{q'}|\frac{N}{2}-1, m_z, k'\rangle = \delta_{k,k'}E_{\text{Dicke}} + \frac{1}{N}\sum_{q\neq q'} J_{q,q'}\left[e^{\frac{2\pi i}{N}(k'-k)q} - e^{\frac{2\pi i}{N}(k'q'-kq)}\right]. \quad \text{(S3)}$$

The Dicke gap is then defined as the difference between the smallest eigenvalue of this matrix and the energy of the Dicke states. As two concrete examples, in the all-to-all case, $J_{q,q'} = J(1-\delta_{q,q'})$, the Dicke gap is $G = JN$, and in the nearest-neighbor case $J_{q,q'} = \delta_{|q-q'|,1}J$, $G = 2(1-\cos(2\pi/N)) \sim \frac{4\pi^2}{N^2} + \mathcal{O}\left(1/N^3\right)$. These examples illustrate the general observation that long-range, near-collective interactions cause the Dicke gap to grow with particle number, while the Dicke gap decreases with N for sufficiently short-range interactions.

In Fig. 7 we show the Dicke gap G for a Heisenberg model with $J_{q,q'} = J^{\perp}_{q,q'}$, where $\mathbb{J}^{\perp}$ corresponds to different realizations of the energy-lattice spin model. The leftmost panel shows the scaling of the gaps at fixed gradient strength with particle number. The gaps are always larger for smaller gradient strength, showing that smaller gradients always lead to a more collective, near-Heisenberg behavior. The rightmost panels show the behavior of the gaps at fixed particle number as a function of gradient strength. For any fixed number of particles, there is a finite critical gradient strength where the Dicke gap closes. This critical gradient decreases with increasing particle number. However, at small enough gradient strengths, the Dicke gap is larger for increasing particle number. This demonstrates that increasing the particle number can either increase or decrease the Dicke gap.

SPIN SEGREGATION

We can quantify spin segregation by the second moment of the spin density $\mu_{2z} = 2\int_{-\infty}^{\infty} dx x^2\langle\hat{\mathcal{S}}^Z(x)\rangle$. For a homogeneous spin distribution, $\mu_{2z} = 0$. When the $\uparrow$ ($\downarrow$) spins are concentrated more towards the edges of the trap, the sign of μ_{2z} is positive (negative). If we only consider dynamics within the Dicke manifold, $\langle\hat{\mathcal{S}}^Z(x)\rangle = 0$ at all times, so we need to examine couplings to other total spin sectors. First we will describe how these terms lead to spin segregation for two particles, and then discuss the many particle generalization. In this analysis we assume that $J^Z_{nm} = J^{\perp}_{nm}$ and inhomogeneities come only from single-particle terms. For two particles the initial state occupies the $S = 1$ (triplet) manifold. The $m_z = 0$ triplet $|t_0\rangle = \frac{1}{2}(|\uparrow\downarrow\rangle + |\downarrow\uparrow\rangle)$ is coupled to the singlet $|s\rangle = \frac{1}{2}(|\uparrow\downarrow\rangle - |\downarrow\uparrow\rangle)$ by the inhomogeneity. Assuming the mode configuation is $\{0, 1\}$ and fixed, the Hamiltonian and spin density in the

$\{|s\rangle,|t_0\rangle,|t_{-1}\rangle,|t_1\rangle\}$ basis are

$$\hat{H} = \begin{pmatrix} -2J_{10}^{\perp}u_{\uparrow\downarrow} & \Delta\omega & 0 & 0 \\ \Delta\omega & 0 & 0 & 0 \\ 0 & 0 & -2\Delta\omega & 0 \\ 0 & 0 & 0 & 2\Delta\omega \end{pmatrix},$$
$$\hat{S}^Z(x) = \frac{1}{2}\begin{pmatrix} 0 & \phi_0(x)^2-\phi_1(x)^2 & 0 & 0 \\ \phi_0(x)^2-\phi_1(x)^2 & 0 & 0 & 0 \\ 0 & 0 & -\phi_0(x)^2-\phi_1(x)^2 & 0 \\ 0 & 0 & 0 & \phi_0(x)^2+\phi_1(x)^2 \end{pmatrix}, \tag{S4}$$

where we have assumed $\phi_n^{\uparrow}(x) = \phi_n^{\downarrow}(x) = \phi_n(x)$, a good approximation for weak gradients. Since the $m_z = \pm 1$ triplets are eigenstates of both the Hamiltonian and observable $\hat{S}^Z(x)$ they do not contribute to the dynamics. $\hat{S}^Z(x)$ measures the spatially-resolved coherence between the $|s\rangle$ and $|t_0\rangle$ states. It follows that $\langle\hat{S}^Z(x;t)\rangle \approx \frac{\omega_B^2}{4J_{10}^{\perp}u_{\uparrow\downarrow}}\sin^2\left(J_{10}^{\perp}u_{\uparrow\downarrow}t\right)\left(\phi_0(x)^2-\phi_1(x)^2\right)$, which exhibits Rabi oscillations.

To understand spin segregation in a many body system we have to consider the coupling of the Dicke states $|N/2,m_z\rangle$ to sectors with different total S. To first order, local spin operators $\hat{\sigma}_n^{\alpha}$ couple the Dicke states to the spin wave states $|N/2-1,m_z,k\rangle$ [25]. We will examine the dynamics within this subspace, assuming the population in the spin wave sector is much smaller than that of the Dicke sector, suppressed by the small parameter $\Delta\omega/u_{\uparrow\downarrow}$. We also assume that the interactions are fully collective for simplicity. We use the matrix elements [25]:

$$\langle N/2,m|\hat{\sigma}_n^Z|N/2-1,m',k\rangle = 2e^{2\pi ikn/N}\sqrt{\frac{(N/2)^2-m^2}{N^2(N-1)}}\delta_{m,m'}$$
$$\langle N/2-1,m,k|\hat{\sigma}_n^Z|N/2-1,m',k'\rangle = \left(2e^{2\pi i(k'-k)n/N}+N\delta_{k,k'}\right)\frac{2m}{N(N-2)}\delta_{m,m'}. \tag{S5}$$

The single-particle inhomogeneity is $\sum_n n\Delta\omega\hat{\sigma}_n^Z$ so it is useful to consider the sums

$$M_{m,k} \equiv \langle N/2,m|\sum_n n\Delta\omega\hat{\sigma}_n^Z|N/2-1,m',k\rangle, \quad P_{m,k,k'} \equiv \langle N/2-1,m,k|\sum_n n\Delta\omega\hat{\sigma}_n^Z|N/2-1,m',k'\rangle. \tag{S6}$$

Writing $|\psi\rangle = \sum_m c_m|N/2,m\rangle + \sum_{m,k} d_{m,k}|N/2-1,m,k\rangle$, the Schrödinger equation implies

$$i\dot{c}_m = Gc_m + \sum_k M_{m,k}d_{m,k}, \qquad i\dot{d}_{m,k} = M_{m,k}^*c_m + \sum_{k'}P_{m,k,k'}d_{m,k}, \tag{S7}$$

where we have re-zeroed the energy. We assume $c_m \gg d_{m,k}$ and use the fact that $P_{m,k,k} \gg P_{m,k,k'}$, for $k \neq k'$, which leads to:

$$c_m(t) \approx c_m(0)\left(1-\sum_k|M_{m,k}|^2\frac{\left(1-e^{-iGt}\right)}{G|G|}\right), \quad d_{m,k}(t) \approx -\sum_{k'}|M_{m,k'}|^2\frac{c_m(0)M_{m,k}^*}{(G)^3}\left(1-e^{-iGt}\right), \tag{S8}$$

implying

$$\langle\hat{S}^Z(x;t)\rangle = \frac{1}{2}\sum_{n,m,k}\left(c_m^*(t)d_{m,k}(t)\langle N/2,m|(\phi_n(x))^2\hat{\sigma}_n^Z|N/2-1,m,k\rangle + \text{H.c.}\right)$$
$$= 2\sum_{n,m,k}(\phi_n(x))^2\sqrt{\frac{(N/2)^2-m^2}{N^2(N-1)}}\text{Re}[c_m^*(t)d_{m,k}(t)e^{2\pi ikn/N}]. \tag{S9}$$

The spin density is proportional to $c_m^*(t)d_{m,k}(t)$ which measures the coherence between the Dicke and spin wave states, which is the many body analogy to the two particle result. We see that the density 1) oscillates at frequency $G \propto u_{\uparrow\downarrow}$, 2) has an inhomogeneous mode dependence which leads segregation in real space, and 3) is $\propto \text{Sign}[G]$ so segregation reverses when interactions are switched from repulsive to attractive. We have assumed $|M_{m,k}|/G$ and $|P_{m,k,k}|/G$ are small parameters. When this condition is not satisfied, interactions can not suppress the single particle dynamics and the initially populated collective Dicke states will be depleted during time evolution.

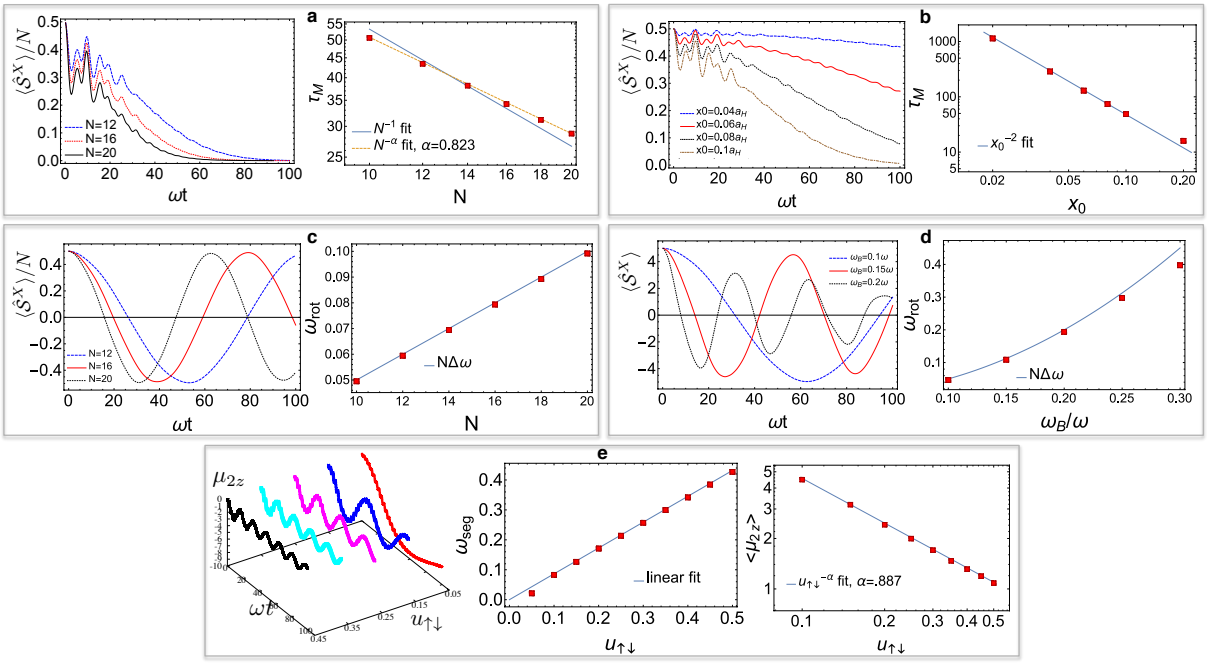

FIG. 8. Scaling. (a) Dynamics vs. N for a constant gradient $x_0 = 0.1a_H$, from which τ_M is extracted and found to scale like $\tau_M \sim N^{-.823}$, close to the N^{-1} prediction. (b) Dynamics and scaling of τ_M vs. x_0 which agrees well with the prediction x_0^{-2}, for $N = 10$. (c) $\langle\hat{S}^X\rangle/N$ vs. N, when $\omega_B = 0.1\omega$, from which ω_{rot} is extracted and agrees well with the prediction $\omega_{rot} = N\Delta\omega$. (d) $\langle\hat{S}^X\rangle$ vs. ω_B for $N = 10$. Predictions fail when $\omega_B \sim u_{\uparrow\downarrow}$. (All cases are $u_{\uparrow\downarrow} = 0.35\omega$.) (e) μ_{2z}, vs. $u_{\uparrow\downarrow}$; oscillations become more pronounced for stronger interactions. ω_{seg} scales linearly with $u_{\uparrow\downarrow}$. $\langle\mu_{2z}\rangle \sim u_{\uparrow\downarrow}^{-.887}$, close to the prediction of $u_{\uparrow\downarrow}^{-1}$.

SCALING OF DYNAMICAL QUANTITIES

The short time dynamics of a generic XXZ Hamiltonian for a state initially polarized along the X direction is [43]

$$\langle\hat{S}^X\rangle = \frac{N}{2} - \frac{(u_{\uparrow\downarrow}t)^2}{32}\sum_{n\neq m}\Delta_{nm}^2 + O(t^3) \approx \langle\hat{S}^X\rangle_{t=0}\left(1-(t/\tau_M)^2\right), \quad \tau_M = 4(Nu_{\uparrow\downarrow})^{-1}\sqrt{\sum_{n\neq m}\Delta_{nm}^2}, \tag{S10}$$

where $\Delta_{nm} \equiv J_{nm}^Z - J_{nm}^\perp$ and τ_M is defined as the demagnetization time. For a linear gradient we expand the parameters in x_0/a_H, set $a_H = 1$, and find $\Delta_{nm} = J_{nm}^Z - J_{nm}^\perp \approx 2x_0^2\Lambda_{nm}$, where

$$\Lambda_{nm} = \Big((n+1)J^0_{n+1,m} - nJ^0_{n-1,m} - \sqrt{n(n+1)}J^0_{n+1,n-1,m,m} - \sqrt{(n+1)(m+1)}J_{n+1,m+1,n,m} + \sqrt{n(m+1)}J_{n-1,m+1,n,m} + \sqrt{(n+1)m}A_{n+1,m-1,n,m} - \sqrt{nm}J_{n+1,m+1,n,m}\Big), \tag{S11}$$

$J^0_{nmpq} = \int_{-\infty}^{\infty} dx\phi_n(x)\phi_m(x)\phi_p(x)\phi_q(x)$, and $J^0_{nm} \equiv J^0_{nnmm}$. The formula $\overline{\Lambda_{nm}} \approx \overline{nJ^0_{nm}} \sim \sqrt{N}$ works well, where $\overline{X_{nm}} \equiv \sum_{n,m\in\mathbf{n}^i} X_{nm}/(N(N-1))$ is the arithmetic average and we have used $\overline{J^0_{nm}} \sim 1/\sqrt{N}$. We find that for $x_0 \ll a_H$, $\overline{\Delta_{nm}} \sim x_0^2\sqrt{N}$. Further assuming $\overline{\Delta_{nm}^2} \approx (\overline{\Delta_{nm}})^2$, this implies $\tau_M \sim \left(Nu_{\uparrow\downarrow}x_0^2\right)^{-1}$. Fig. 8(a) shows the scaling of τ_N vs. N. Fitting the dynamics to a Gaussian decay function $A\exp(-t^2/\tau_M^2)$ we find that $\tau_M \sim N^{-.823}$, close to the prediction of N^{-1}. In Fig. 8(b) we show the scaling of τ_M vs. x_0, which agrees well with the x_0^{-2} prediction.

In Fig. 8(c,d) we show how $\langle\hat{S}^X\rangle$ depends on N and ω_B, respectively. We use a cosine fitting function $A\cos(\omega_{rot}t)$ to extract the collective Bloch vector precession frequency ω_{rot} and compare with the prediction $N\Delta\omega$. In Fig. 8(c) we use $\omega_B = 0.1\omega$ and a relatively large interaction strength $u_{\uparrow\downarrow} = 0.35\omega \gg \Delta\omega$. This is the self-rephasing regime so the prediction works well. In Fig. 8(d) we fix $N = 10$ and $u_{\uparrow\downarrow} = 0.35\omega$, and vary ω_B. We see deviations from the prediction for large ω_B, because interactions are not strong enough to protect against population leakage outside of the Dicke manifold. In Fig. 8(e) we plot μ_{2z} dynamics for various interaction strengths, fixing $N = 10$ and $\omega_B = 0.1\omega$.

For larger interactions the oscillations become smaller, faster, and less damped, confirming the "Rabi oscillation" behavior of spin segregation. We fit μ_{2z} to an offset cosine function $A + B\cos(\omega_{seg}t + \phi)$ to extract the scaling of the segregation frequency ω_{seg}, and the average value of the segregation, $\langle\mu_{2z}\rangle = A$. A linear fit of ω_{seg} vs. $u_{\uparrow\downarrow}$ with slope of 0.86 confirms linear scaling with interaction energy. We find $\langle\mu_{2z}\rangle \sim u_{\uparrow\downarrow}^{-0.887}$, close to the prediction of $u_{\uparrow\downarrow}^{-1}$.

MATRIX PRODUCT STATE SIMULATIONS

The variational matrix product state (MPS) studies of the main text were performed using extensions of the open source MPS library [62, 63]. We use an MPS anstaz which explicitly conserves total particle number, but does not conserve the total magnetization. While the dynamics preserve the total magnetization, the initial collective rotation of spins along the x direction involves a sum over many different magnetization sectors, and so leaving the magnetization unconstrained is convenient. Following this collective rotation, the next step is to enact the sudden quench of trapping parameters, which amounts to applying a spin-dependent displacement ($\psi(x) \to \psi(x+\lambda)$, constant gradient) or spin-dependent dilation ($\psi(x) \to \sqrt{\lambda}\psi(\lambda x)$, linear gradient) to the single-particle states. Since we assume harmonic traps, the displacement and dilation operators are known analytically as

$$\begin{aligned}\hat{U}_{\text{displacement}} &= e^{\left(\hat{a}-\hat{a}^\dagger\right)\lambda/(\sqrt{2}a_H)}, \\ \hat{U}_{\text{dilation}} &= e^{\ln\lambda\left(\hat{a}^2-(\hat{a}^\dagger)^2\right)/2},\end{aligned} \tag{S12}$$

where $\hat{a}$ and $\hat{a}^\dagger$ are the ladder operators of the original (no gradient) harmonic oscillator. Writing these ladder operators in second quantized form on the energy lattice, the basis transformations above take the form of time evolution under a hopping model with spin-dependent and inhomogeneous hopping amplitudes. Here, time evolution refers to the fact that the operation consists of applying the exponential of an anti-Hermitian many-body operator. In the constant gradient case, the hopping model contains only nearest-neighbor hopping, while the linear gradient case is a model with only next-nearest neighbor hopping. We enact this effective time evolution by decomposing it into a product of few-site unitaries using a Trotter decomposition with the error controlled by a small "step size" $\Delta\lambda$, and then applying these few-site unitaries to the MPS via standard techniques [31].

Next, we wish to perform time evolution under the long-range spin model

$$\begin{aligned}\hat{H} = &\frac{u_{\uparrow\downarrow}}{4}\sum_{n\neq m}\left[J^Z_{nm}\left(\hat{N}_n\hat{N}_m - \hat{\sigma}^Z_n\hat{\sigma}^Z_m\right) - J^\perp_{nm}\left(\hat{\sigma}^X_n\hat{\sigma}^X_m + \hat{\sigma}^Y_n\hat{\sigma}^Y_m\right) + \frac{1}{2}\left(J^Z_{nm} - J^Z_{mn}\right)\left(\sigma^Z_n\hat{N}_m - \sigma^Z_m\hat{N}_n\right)\right] \\ &+u_{\uparrow\downarrow}\sum_n J_{nn}\hat{N}^\uparrow_n\hat{N}^\downarrow_n + \sum_n\left[\bar{\omega}(n+1/2)\hat{N}_n + \Delta\omega\,(n+1/2)\,\hat{\sigma}^Z_n\right],\end{aligned} \tag{S13}$$

where $J_{nn} \equiv A_{nnnn}$. We perform time evolution using the second-order method of Zaletel *et al.* [66]. In this method, an explicit matrix product operator (MPO) approximation to the propagator $\hat{U}$ is formed from the MPO form of the Hamiltonian, which is then applied to the state at time t, $|\psi(t)\rangle$ by variational minimization of the functional $\left||\phi\rangle - \hat{U}|\psi(t)\rangle\right|^2$ over all MPSs $|\phi\rangle$ with fixed resources. For the variational minimization, we perform four sweeps per timestep and impose an upper limit on the discarded weight per bond of 10^{-9}. The maximum bond dimension used in the simulations of this work is roughly 2000.

In order to apply the method of Zaletel *et al.*, we must construct an MPO representation of the Hamiltonian Eq. (S13). For long-range interactions which are translationally invariant, $\hat{H} = \sum_{i<j} f(j-i)\,\hat{A}_i\hat{B}_j$, a well-established procedure exists for converting this interaction into an MPO [67, 68]. In this procedure, the function $f(r)$ is fitted to a sum of n_{exp} exponentials via the ansatz $\tilde{f}(r) = \sum_{n=1}^{n_{\text{exp}}} J_n\lambda_n^r$, and then a known MPO construction of exponentially decaying interactions is used. Interactions on the single-particle mode space lattice are not translationally invariant, and so this procedure does not apply. However, we have devised a related procedure, in which an inhomogeneous interaction $\hat{H} = \sum_{i<j} f(i,j)\,\hat{A}_i\hat{B}_j$ is modeled by a sum of exponentials with site-dependent weights and exponential decay parameters via the ansatz $\tilde{f}(i,j) = \sum_{n=1}^{n_{\text{exp}}} J_{i,n}\prod_{k=i}^{j-1}\lambda_{k,n}$. These parameters are variationally optimized using an alternating least squares algorithm. Imposing the condition that the residual $\sum_{i<j}\left|f(i,j) - \tilde{f}(i,j)\right|^2 < 10^{-7}$ leads to approximations with $n_{\text{exp}} \sim 7$ exponentials.